


## Research

# A fuzzy path analysis of the impact of urban infrastructure planning on land surface temperature

Elham Sanagar Darbani<sup>1</sup>  · Danial Monsefi Parapari<sup>2</sup>  · Shady Attia<sup>3</sup>  · Ehsan Sharifi<sup>1</sup> 

Received: 4 September 2024 / Accepted: 10 February 2025

Published online: 25 February 2025

© The Author(s) 2025 

## Abstract

The urban heat island (UHI) effect is one of the most studied manifestations of urban climate in cities. Understanding the dynamics of UHIs and identifying their relationship with changes in urban landscape and infrastructure is necessary to address tailored adaptation and mitigation policies. This paper aims to explore the effects of urban infrastructures (UI) on land surface temperature (LST) and the energy balance. The land surface temperature is retrieved via the split-windows method. To calculate the urban infrastructure relationships with land surface temperature, the impact of urban infrastructures and urbanization on LST is analyzed using Getis Ord Gi\* statistics and Band Collection Statistics (BCS). Fuzzy Path analysis is used to evaluate the coefficient values of each urban infrastructure (green–blue–gray–red) with LST in the case study of Mashhad. Results indicate that (a) urban gray infrastructure (UGRI), urban red infrastructure (URI), and urban blue infrastructure (UBI) have a direct impact on LST, (b) the urban green infrastructure (UGI) can have a diverse impact on LST, (c) among the urban infrastructures, the urban gray infrastructure has the highest and urban red infrastructure has lowest impact on LST. Findings highlight the vital need for contextual policies for UHI mitigation strategies tailored to the urban grey infrastructure. The methodology used in this paper can be evaluated in other cities worldwide.

**Keywords** Urban infrastructure · Land surface temperature · Urban greenery · Fuzzy path analysis

## Abbreviations

LST	Land surface temperature
UI	Urban infrastructure
UHI	Urban heat island
UGI	Urban green infrastructures
UGRI	Urban gray infrastructures
UBI	Urban blue infrastructures
URI	Urban red infrastructures
LUC	Land-use cover
AT	Air temperature
BCS	Band collection statistics

**Supplementary Information** The online version contains supplementary material available at <https://doi.org/10.1007/s44327-025-00049-3>.

✉ Elham Sanagar Darbani, Elham.Sanagardarbani@Adelaide.edu.au; Danial Monsefi Parapari, parapari@shahroodut.ac.ir; Shady Attia, shady.attia@uliege.be; Ehsan Sharifi, Ehsan.sharifi@adelaide.edu.au | <sup>1</sup>School of Architecture and Civil Engineering, University of Adelaide, Adelaide, Australia. <sup>2</sup>Shahrood University of Technology, Shahrood, Iran. <sup>3</sup>Sustainable Building Design Lab, Dept. UEE, Faculty of Applied Sciences, University of Liège, Liège, Belgium.



SVF Sky view factor  
BCR Building coverage ratio

## 1 Introduction

With the global population projected to rise to 9.7 billion by 2050 [1], rapid urban expansion has become inevitable. This population surge places substantial demands on urban infrastructure and critical ecosystem services within cities. However, urban expansion often leads to a degradation in ecosystem services [2], resulting in environmental challenges that affect urban life quality and sustainability. For instance, cities across East Asia have experienced large-scale infrastructure growth, leading to the Urban Heat Island (UHI) effect, which is linked to elevated surface and air temperatures in urban areas compared to surrounding rural environments [3]. The UHI effect exacerbates energy demand in cities, where increased cooling needs drive up energy consumption. This increased demand not only affects indoor thermal comfort but also adds to outdoor heat stress [4–7], generating higher levels of pollutants such as sulfur dioxide, carbon monoxide, nitrogen oxides, and particulate matter from power generation sources reliant on fossil fuels [8].

The impact of UHI can be studied through Land Surface Temperature (LST), a critical metric for assessing surface heat distribution and the energy exchange dynamics on urban surfaces [9, 10]. LST plays a significant role in determining urban air quality [11], thermal comfort [12], human health [13], energy consumption [14, 15], and even water quality [16]. Equation 1 outlines the relationship between UHI intensity and the urban land surface energy budget [17], showing that surface characteristics, like albedo, can influence how much solar radiation is absorbed or reflected by urban surfaces. Consequently, surfaces with higher albedo reduce solar radiation retention, mitigating the UHI effect to some extent.

$$(1 - \alpha)I_{\downarrow} + I_{\downarrow}(LW) - \epsilon\sigma T_s^4 - H_s - H_l - H_g = 0 \quad (1)$$

where  $\alpha$ ,  $\epsilon$  and  $T_s$  are the surface albedo, emissivity and temperature,  $I_{\downarrow}$  is the downward surface insolation,  $I_{\downarrow}(LW)$  is the downward long-wave radiation,  $\sigma$  is the Stefan Boltzmann constant,  $H_s$  and  $H_l$  are the sensible and latent heat fluxes and  $H_g$  is the ground heat flux.

Given these connections, understanding how various types of urban infrastructure (UI) contribute to LST is critical. UI encompasses a range of elements fundamental to urban functionality, which can be broadly categorized into human-centered aspects and physical components. Human-centered UI includes structures supporting a city's economic, social, and political systems [18–21], whereas physical UI comprises the built environment, such as buildings, transportation systems, and green spaces [22, 23]. Different infrastructure types influence LST and contribute to UHI in unique ways.

Urban green infrastructure (UGI), for example, has been recognized as an effective means of mitigating climate change impacts within cities. By enhancing urban sustainability and resilience, UGI helps counteract the UHI effect through shading, evapotranspiration, and improved air quality [24–35]. Similarly, urban blue infrastructure (UBI)—which includes natural and artificial water bodies—plays a significant role in moderating UHI intensity by emitting longwave radiation to cool urban surfaces, particularly during high-temperature periods [36–41]. Urban gray infrastructure (UGRI), consisting of the engineered structures that shape city form and function, also affects LST, but its impacts are often less straightforward to categorize due to overlapping elements like mixed-use spaces [28, 42–45].

Recent studies have explored the interactions between Land Surface Temperature (LST) and Urban Infrastructures (UI). This research builds on previous works examining UI and LST and their effects on urban energy balance, using Mashhad as a case study. However, the influence of Urban Red Infrastructures (URI) on LST has been overlooked. URI is the human infrastructure that creates an environment providing functions for the social, economic, and political systems [46] (Table S1). The overall view of the UI in a city with examples, is shown in the Table 1. Since previous studies have not identified the specific factors of URI, this research aims to determine these factors through interviews and questionnaires with urban experts to identify the URI components affecting LST in Mashhad.

Moreover, although a few related studies have particularly explored LST in Mashhad [47, 48], there are still several challenges to be further improved including the impact of UI on LST. The increase in air temperatures, not only affects urban energy usage intensity, but also leads to significant growth of heat related diseases and mortality in summer [49]. This paper aims to answer two key research questions: (A) What are the specific effects of urban infrastructure (UI) on land surface temperature (LST) and energy balance? and (B) How do interactions among green, blue, grey, and red infrastructures influence LST? The study presents a structured methodology to evaluate how different UI components interact with LST. Additionally, it introduces a novel approach for quantifying the significance of these interactions within

**Table 1** Categories of Urban Infrastructure (UI) with Examples

Category	Examples
UGRI	Roads, streets, bridges, transportation systems, sewage systems
UGI	Parks, urban forests, gardens
UBI	Rivers, lakes, canals, reservoirs
URI	People and families per residential Unit

the current urban framework and their potential impact on future urban developments. Given that urban planning regulations are consistent across Iranian cities, this methodology can be broadly applied to identify UI parameters that affect LST and energy balance in other urban settings as well. This is because cities in Iran follow similar planning frameworks, infrastructure types, zoning practices, and building standards are largely consistent nationwide. This regulatory uniformity ensures that the interactions between various UI and LST observed in one city are likely to be applicable to others with similar urban forms and densities.

## 2 Materials and methods

### 2.1 Study area

This study is conducted in Mashhad, the capital city of Khorasan-e-Razavi province, located in the northeast of Iran ( $36^{\circ}37'–36^{\circ}58'N$ ,  $59^{\circ}26'–59^{\circ}44'E$ ) with a population of 3,057,679 according to the Statistical Centre of Iran in 2016 (Fig. 1a). Mashhad is the second most populous city of this country, with 13 municipal districts. According to the Köppen classification system, this city has an arid climate with hot summers and cool winters. It experienced a mean temperature of  $26.74^{\circ}C$  in June, and  $28.81^{\circ}C$  in July during 2007–2017. According to the Mashhad meteorological weather website, Mashhad has high air temperature exceeding  $40^{\circ}C$  in summer, dropping to the average minimum temperature of  $-4.8^{\circ}C$

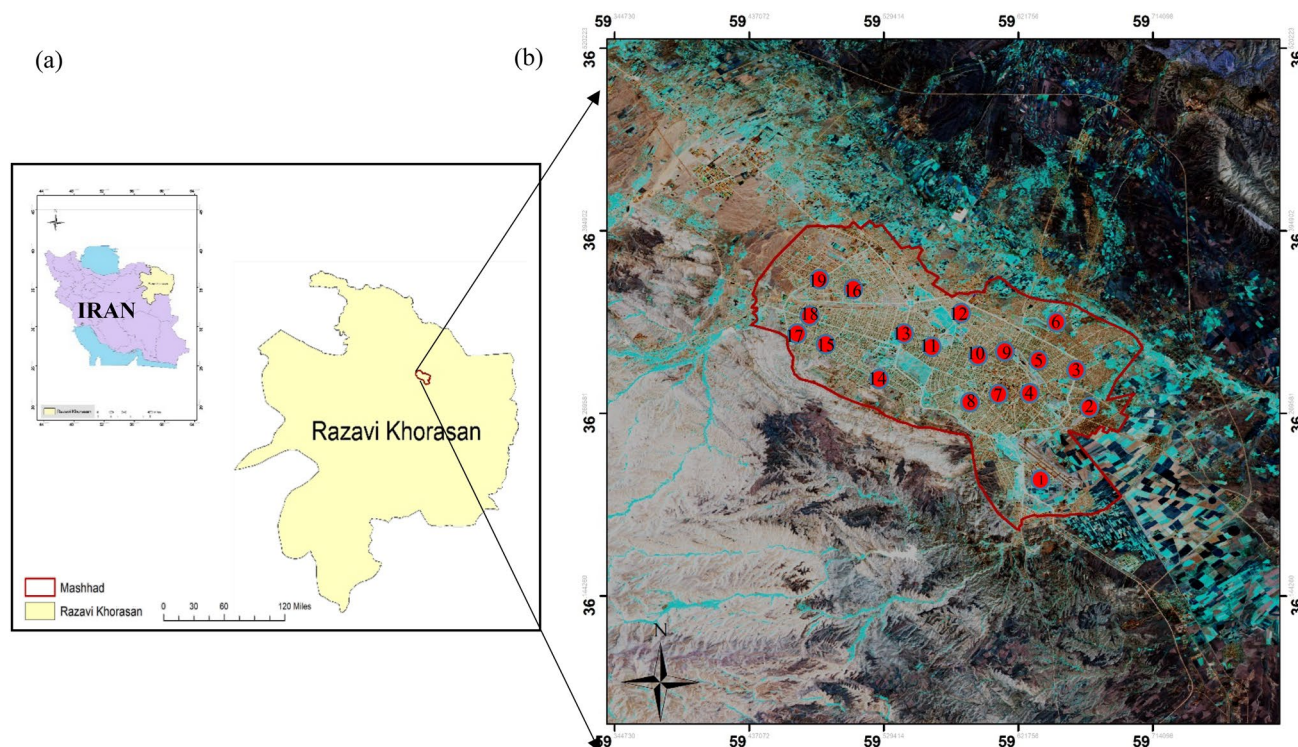


**Fig. 1** **a** Location of Mashhad in northeast of Iran and map of the study area, the image is a Landsat 8 image with band 5, 4, and 3 in RGB on July 22, 2022. **b** Meteorological stations

in winter. A study of wind direction determines that the dominant wind direction is eastern while the gulf wind blows from the south. Spring has high precipitation (248.92 mm on average), while summer is quite dry. Meteorological data during the decade from 2007 to 2017 for Mashhad shows that the relative humidity of the city has been decreasing, while between 2016 and 2017 this movement is fluctuating. During these years, the air temperature trend has shown an upward trend. June, July and August are the warmest months, with a mean temperature of 28.41 °C, while January, February and December are the coldest months with a mean temperature of 6.5 °C. A study of the development of Mashhad over the past thirty years shows that along with the population growth (including refugees and undocumented immigrants), the rate of development of the city has been significant; and has increased nearly sevenfold during only one decade. An important part of this increase is related to the 80's rapid urbanization and uncontrolled immigration, which included both internally displaced people and Afghan asylum seekers. Since 1980, the population of Mashhad has more than doubled [50]. In Mashhad, the LST increased over the period of approximately 30 years [47].

## 2.2 Land-use classification

In this research, the legal boundary of Mashhad, which was approved by Mashhad Municipality in 2015, has been used alongside the latest Mashhad GIS database, published in 2021 (Fig. 2). Since in this climate (BSk), the effects of climate change in summer are much more severe on human health, the study is focused on summer. Figure 2a shows the area (he) of the main land uses in Mashhad, which are classified in eleven categories. As depicted in Fig. 2b, residential areas and agricultural lands have the highest percentage of land use (7715 he and 4521.09 he). Green spaces in Mashhad include gardens, parks and grass lands.

## 2.3 Data analysis

The LST map of Mashhad was prepared using the split-window algorithm [51]. The time frame selected for this analysis is the summer of 2022, which was analyzed using the Moran coefficient and the hotspot method, as well as the Band Collection Statistics (BCS) method. As the lower grid size brings better model estimation [52] we used 30 m grid size. Indicators of UI that affect urbanization in Mashhad were identified from literature review and interviews, and with questionnaire and snowball sampling (250 questionnaires) we evaluated those indicators which have an impact on LST. Out of 85 relevant indicators (Table S1 in supplementary file-SF), 35 were removed due to lack of accessible data in Mashhad. Additionally, 15 further indicators that had low  $p$  were also removed. The selected indicators needed to be actionable for urban planning purposes. We aimed to retain those that could provide valuable insights for policymakers and urban planners, ensuring the study's relevance to real-world applications. The remaining 32 combined indicators were examined further (Table 2). The effect of these indicators on different categories of UI and the intensity of LST are further explored by regression analysis. By applying regression analysis, we aimed to quantify the strength and direction of the influence that UI have on LST. This method allows us to identify which indicators significantly impact LST changes. The results of the regression analysis are presented with corresponding coefficients,  $p$ -values, and  $R^2$  values, which indicate the predictive power and significance of the relationships identified. The coefficient of impact of each UI on LST was calculated through path analysis. Building on the results from the regression analysis, path analysis further investigates the direct and indirect relationships among multiple variables. This method allows us to understand the complex interactions between UI and LST by creating a model that maps these relationships. Three data sources were considered in this study including Landsat 8, SAGA-GIS [53] model and local GIS data, provided by municipality of Mashhad. The selection of Landsat 8 and SAGA-GIS as data sources for analyzing Land Surface Temperature (LST) in Mashhad is based on their specific capabilities and relevance to urban thermal analysis. Landsat 8 offers high-resolution thermal imaging, which is essential for accurately capturing surface temperature variations across urban areas. Its thermal bands are specifically designed to measure LST, providing reliable data that reflects the complex interactions within the urban environment. Additionally, SAGA-GIS is utilized for its robust spatial analysis tools, allowing for efficient processing of the Landsat data. The software's ability to integrate various datasets enhances the analysis of LST in relation to different urban infrastructure types. SAGA-GIS is recognized for its effectiveness in operating GIS, ensuring that the analytical approach.

In this study, ArcGIS was employed and the models, algorithms and images of Landsat 8 (OLI) satellite [58] were used for summer 2022 (Fig. 2b and Table 3). The image was chosen for the hottest day with the help of nearest meteorology station, in Mashhad airport. The satellite image was considered with minimal cloud coverage. The Landsat data was obtained at <https://earthexplorer.usgs.gov> that is provided by NASA and data is recorded at 100m and resampled to 30m.



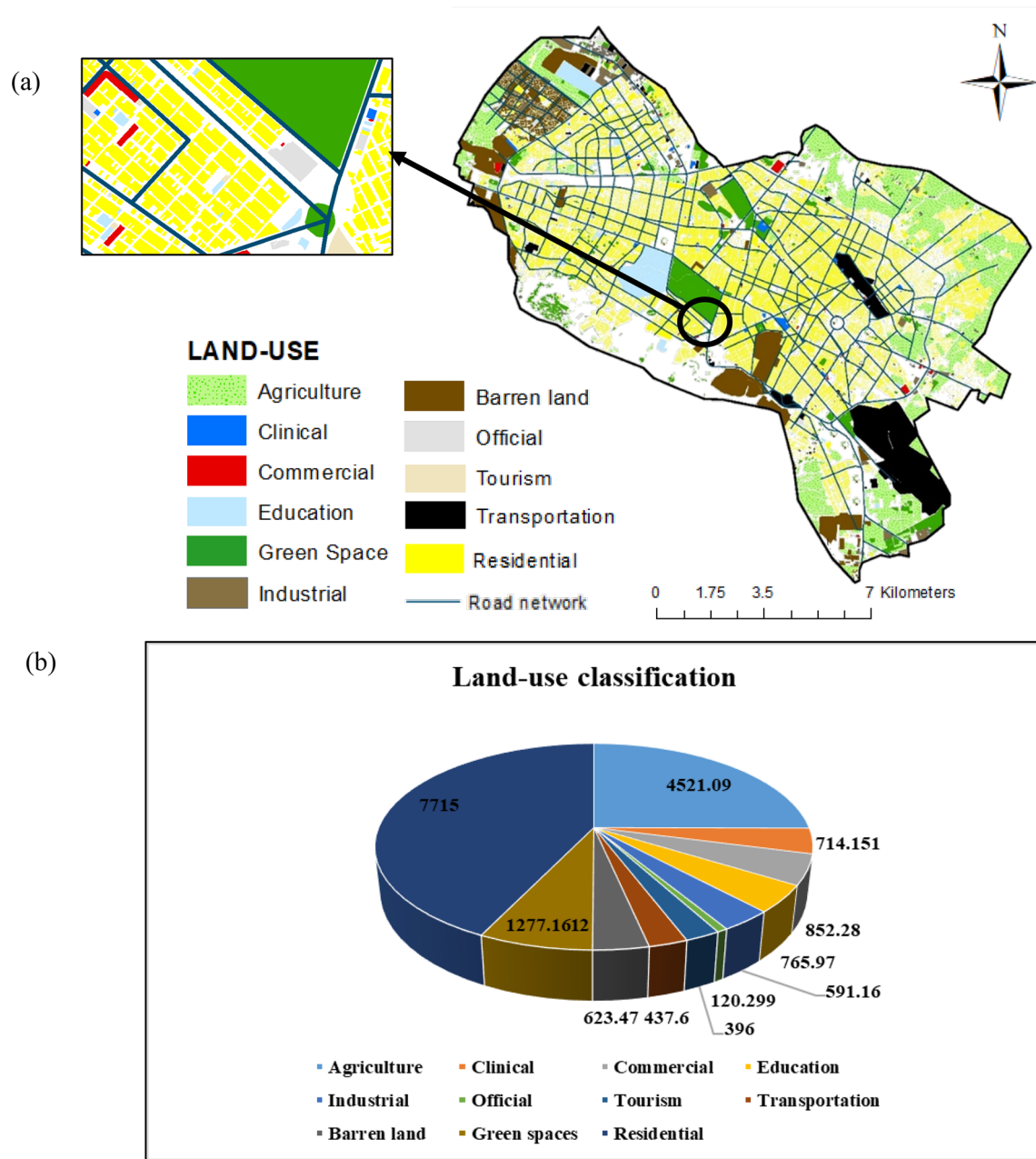


**Fig. 2** **a** Spatial distribution of land uses in the Mashhad, **b** the land-use area (he)

## 2.4 Land surface temperature retrieval

Table S2. In supplementary section shows all parameters that were used to estimate the LST of Mashhad using Landsat 8 images in 2022. Atmosphere has always been an influential factor in remote sensing and because of its function, the numerical value of each pixel in remote sensing images is not a true record of the radiance of surface phenomena. This is because the signals are attenuated by absorption or changed by scattering. Atmospheric corrections are applied according to time and geographical location before calculating LST [48]. The Chavez method was used for atmospheric correction to correct atmospheric errors. This method works in such a way that the minimum numerical value of one pixel for the blue zones in each band must be zero, otherwise this value is based on atmospheric error (Eq. 2 and Eq. 3)[59].

$$L = \text{Gain} \times \text{DN} + \text{offset} \quad (2)$$

**Table 2** Used indicators for evaluating the effect of UI on LST variation

Urban Infrastructure	Indicator	Formula	Description	Data Source
UGI	Green spaces	Area	The areas allocated for gardens and parks, constructed by the municipality and used by the public	GIS layer
	NDVI	$NDVI = (\rho_{nir} - \rho_{red}) / (\rho_{nir} + \rho_{red})$	NDVI is the density of vegetation [54] which is calculated by the equation: The NDVI value of each pixel is a number between -1 and 1, with values greater than 0 indicating vegetation cover and higher values signify denser green lands	Landsat 8
	NDMI	NDMI is calculated as a ratio between the NIR and SWIR values. NDMI is calculated by equation	NDMI is used to determine vegetation water content	Landsat 8
	NDWI	$NDWI = (Green - NIR) / (Green + NIR)$	NDWI is used for water bodies' analysis [55, 56]. The index uses green and near infra-red bands of remote sensing images. Higher NDWI values demonstrate sufficient moisture while a low value indicates water stress	Landsat 8
UBI	water well	Number	A water well is a pit that is dug to reach subsurface water reservoirs. This method is used for cities in arid climate	GIS layer
	Seasonal river	Length/width/number/areas	Seasonal rivers are rivers that only flow during the rainy season. The rest of the year they can be completely dry	GIS layer
	water distribution system	Length/width/number/areas	A water distribution system is a part of water supply network with components that carry potable water from a centralized treatment plant or wells to water consumers in order to satisfy residential, commercial, and industrial and firefighting requirements	GIS layer
	Population density	$POP_{density} = P_i / A_i$ $P_i$ : population in pixel; $A_i$ : area (hectare)	Population density per pixel	Iranian censuses
URI	Household quantity	$I = P_i / F$ $P_i$ : population in pixel; $F$ = The average household size 3.8 for Mashhad	A family is made up of several people who live together, spend time together, and usually eat together. A person living alone is also considered a household	
	Household size	$L_r = P_i / H$ $P_i$ : population in pixel; $H$ = the number of people per residential unit	The density of people in a residential unit is one of the major indicators of living standards	

**Table 2** (continued)

Urban Infrastructure	Indicator	Formula	Description	Data Source
UGI (land-use-function)	Agriculture	Area	Land allocated to agricultural purposes	GIS layer and Landsat 8
	Clinical	Area	Land dedicated to human and animal health services and social services, including hospitals, clinics, etc	
	Commercial	Area	Commercial land can be any plot or section of land used for commercial purposes and intended to generate a profit	
	Education	Area	Land allocated for formal and public education activities under the management of the Ministries of Education, Labor and Social Affairs, Including kindergarten, elementary school, high school and university	
	Industrial	Area	land used for commercial establishments, manufacturing plants, public utilities, mining, distribution of goods or services	
	Official	Area	Land designated for the establishment of ministries, government agencies, government companies, and public non-governmental organizations and institutions, law enforcement and mobilization. Including institutions, army, ministries, municipalities, etc	
	Tourism	Area	Land allocated for accommodation and tourism	
	Transportation	Area	Land allocated for urban, suburban travel E.g., airports, railways, terminals	
	Barren land	Area	Refers to vacant lands with bare soil or rock	
	Residential	Area	Refers to lands allocated for habitation	
	Road networks	Length/width	The road network is the system of interconnected roads designed to accommodate wheeled road going vehicles and pedestrian traffic	
	Electricity distribution system	Length/width/area/number	Electric power distribution is the final stage in the delivery of electric power and carries electricity from the transmission system to individual consumers	

Table 2 (continued)

Urban Infrastructure	Indicator	Formula	Description	Data Source
UGRI (urban physical)	NDBI	$NDBI = (bni - bmi) / (bni + bmi)$	NDBI describes the built-up density of any geographic area. It is calculated as the ratio between short wave infrared (SWIR) and near infrared (NIR) and have indices range from -1 to 1. Positive numbers show built-up areas. Bni and bmi are the digital numbers of mid-infrared and near-infrared bands of the Landsat images, respectively	Landsat 8
	Sky View Factor (SVF)	$SVFg = [1 + \left(\frac{H^2}{W}\right)^{\frac{1}{2}}]^{-1} - H/W$	The SVF of the mid-width of the floor of a street canyon with symmetric cross-section and infinite length [57]	GIS and Landsat 8
	Building's height	–	–	GIS layers
	Building Coverage Ratio (BCR)	$BCR = (\sum S) / A$ S: The mass of building; A = parcel	Building coverage ratio	–
	Clay material	–	Clay is a type of fine-grained natural soil material	GIS layers
	Brick material	–	A brick is a type of block used to build walls, pavements and other elements in masonry construction	–
	Concrete material	–	A cement is a binder, a substance used for construction that sets, hardens, and adheres to other materials to bind them together	–
	Stone material	–	the types of stone used (e.g., granite, limestone, or sandstone), their natural durability, common applications in construction (such as building facades or pavements), and any notable physical properties like weather resistance or thermal mass	–
	Brick and stone material	–	the advantages of blending these materials, such as enhanced durability or visual appeal	–



**Table 3** Details of Landsat 8 OLI images

Date of Image	Sensor	Resolution (meters)	Temperature (°C)	Cloud cover	Path/Row	Source
22 Jul 2022	OLI (Operational Land Imager) and TIRS (Thermal Infrared Sensor)	(30)	34.56	0:00	159/35	<a href="https://earthexplorer.usgs.gov">https://earthexplorer.usgs.gov</a>

where  $L$  is Spectral Band Radiation,  $DN$ - Digital pixel value (0 to 255), Gain and Offset sensor calibration coefficients.

$$\rho^{\lambda} = (\pi L_{\lambda}) / (ESUN_{(\lambda)} \cos \theta d_r) \quad (3)$$

$\rho^{\lambda}$ : Reflectivity of each band between 0 and 1,  $ESUN_{(\lambda)}$ : Average solar radiation for each band,  $\theta$ : the angle of the solar radiation,  $d_r$ : Inverse square ratio of the distance of the earth to the sun. LST map was produced in ArcGis10.3 for the year 2022 (Fig. 3, Table S2 in Supplementary File- SP).

## 2.5 Hot spot analysis using Getis Ord Gi\* statistics

*Moran's I* is a measure of spatial autocorrelation [60], that is characterized by a correlation in a signal among nearby locations in space. Spatial autocorrelation is more complex than one-dimensional autocorrelation because it is multi-dimensional (i.e., 2 or 3 dimensions of space) and multi-directional. *Moran's I* is defined as:

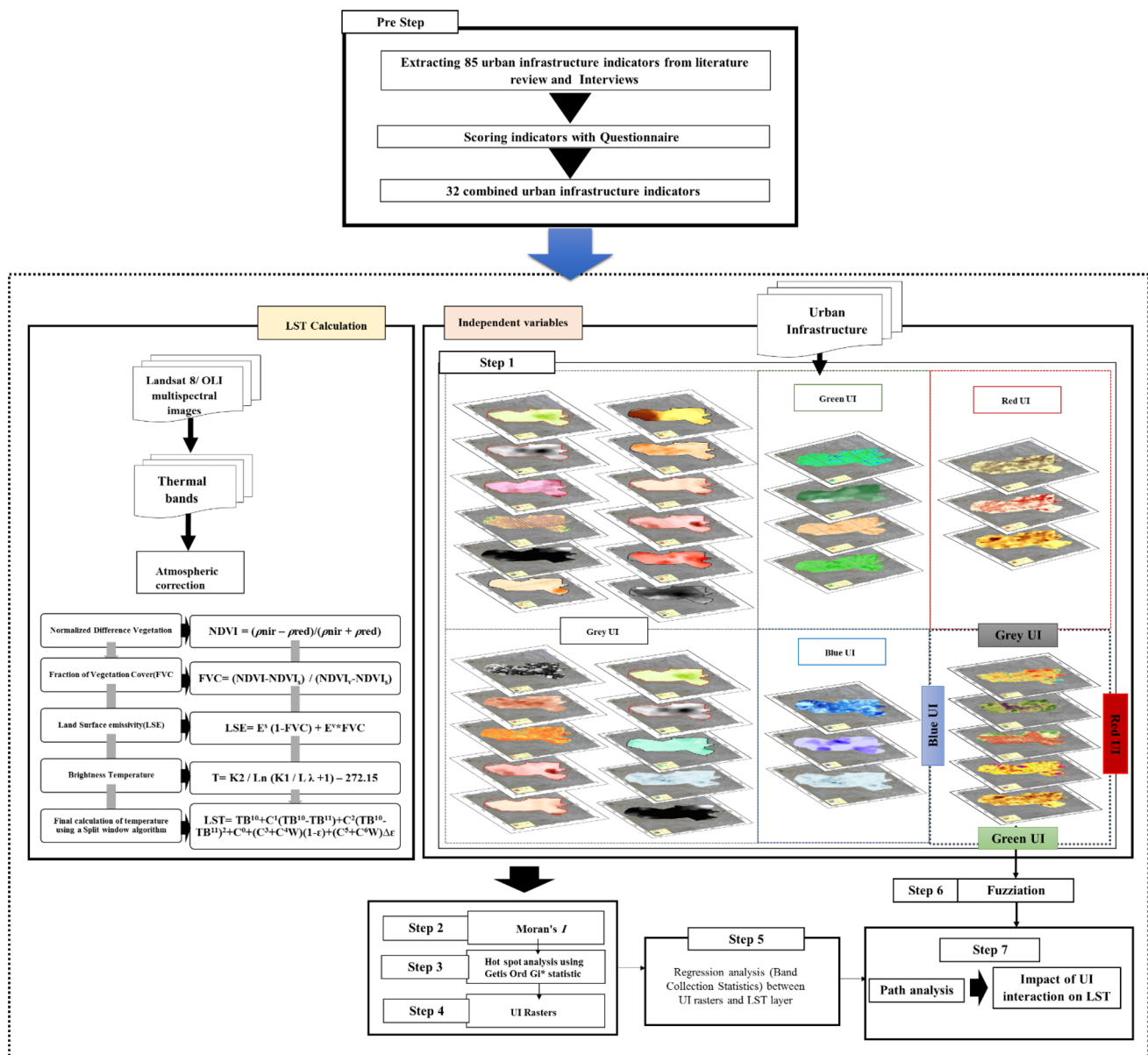


Fig. 3 Flowchart process

$$I = N/w \left( \sum_{(i)} \right) \sum_{(j)} w_{ij} ((x_i) - (x)) (x_j - (x)) / \left( \sum_{(i)} (x_i) - (x) \right)^2 \quad (4)$$

where  $N$  is the number of spatial units indexed by  $i$  and  $j$ ;  $x$  is the variable of interest;  $((x))$  is the mean of  $x$ ;  $w_{ij}$  is a matrix of spatial weights with zeroes on the diagonal (i.e.,  $w_{ii} = 0$ ); and  $W$  is the sum of all  $w_{ij}$ .

Getis-Ord  $G_i^*$  statistical hotspot analysis tool in the ArcGIS software has been used to study the spatial cluster of high and low value features. A high-value complication may not be a statistically significant hotspot. A complication is statistically significant for a statistically significant hotspot surrounded by other high-value complications. The sum of the issues for one complication and its neighbors can be compared to all complications; when the positional sum is very different from the expected total sum, and when the discrepancy is too large for the result to be random. The z-score results are statistically significant. Getis-Ord calculations are statistically derived from the following equation [61]:

$$[G_i]^* = \left( \sum_{(j=1)}^n \right) \left[ w_{(ij)} x_i - X \sum_{(j=1)}^n w_{(ij)} \right] / \left( s \sqrt{ \left( \left[ n \sum_{(j=1)}^n \right] \left[ w_{(ij)} - \left( \sum_{(j=1)}^n \right) \left[ w_{(ij)}^2 \right] \right] (n-1) \right) } \right) \quad (5)$$

where  $x_j$  is the characteristic value of complication  $j$ ,  $w_{(i,j)}$  is the spatial weight between complication  $i$  and  $j$ .  $n$  is equal to the total number of complications.

$$(X) = \sum_{(j=1)}^n [x_j] / n$$

And

$$s = \sqrt{ \left( \left( \sum_{(j=1)}^n x_j^2 \right) / n - ((X)^2) \right) }$$

The Moran coefficient provides insights into spatial autocorrelation, revealing how LST values cluster geographically in relation to UI. A high Moran coefficient indicates that similar LST values are concentrated in specific areas, which may suggest an influence from nearby urban features. The hotspot method identifies regions of significantly elevated or reduced LST, allowing for the detection of critical areas that may require attention in urban planning. For example, areas lacking sufficient UGI are likely to emerge as hotspots of high temperature, highlighting opportunities for intervention.

The output of the  $G_i^*$  statistic returned for each feature in the dataset is a z-score. Higher positive z-score shows more intense clustering of high values (hot spot) and a smaller negative z-score represents more intense clusters of low values (cold spot). The z-score represents the statistical significance of clustering for a specified distance (90% significant:  $> 1.65$  or  $< -1.65$ ; 95% significant:  $> 1.96$  or  $< -1.96$ ; 99% significant:  $> 2.58$  or  $< -2.58$ ; 99.9% significant:  $> 3.29$  or  $< -3.29$ ). At a significance level of 0.05 (95%), a z-score would have to be less than  $-1.96$  or greater than  $1.96$  to be statistically significant. From the statistical results, the LST pattern was divided into seven categories: very hot spot, hot spot, warm spot, not statistically significant, cool spot, cold spot, and very cold spot. In the final statistics of the hot spots and cold spots in our paper, values at 95% or higher confidence level were included. To assess the impact of UI on the LST, the hotspot pattern change was linked to UI layer. This method gives a better demonstration of the LST, rather than focusing only on the high or low LST absolute values separately.

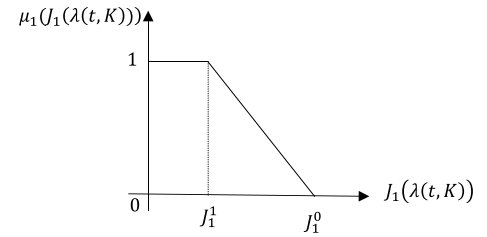
## 2.6 Deriving relationships between factors and LST

In this part of the analysis, according to the theoretical framework and conceptual model of research depicted in Fig. 3 and collection of indicators and available information, four sections of green, blue, gray and red infrastructure have been identified as the main dimensions of indicators affecting the thermal energy of urban surfaces. In the analysis process, target indicators of the mentioned dimensions, raster and spatial maps were produced. The basis of production of these layers of analysis, which has different scales according to the information source, is the degree of correlation. Then, by measuring the spatial correlation using BCS technique, surface thermal energy is estimated in the city.<sup>1</sup> In this technique, the amount and type of association of each of the indicators were determined.

The BCS tool provides statistics for the multivariate analysis of a set of raster bands. When using the compute covariance and the correlation matrices option is enabled, the covariance and correlation matrices are produced as well as the basic statistical parameters, such as the values of minimum, maximum, mean, and standard deviation for each layer. The

<sup>1</sup> www.pro.arcgis.com.

**Fig. 4** membership function for linear condition



remaining entries within the covariance matrix are the covariances between all pairs of input rasters. The following Eq. 6 is used to determine the covariance between layers  $i$  and  $j$ :

$$[Cov]_{ij} = \left( \sum_{k=1}^N [(Z_{ik} - \mu_i)(Z_{jk} - \mu_j)] \right) / (N - 1) \quad (6)$$

$Z$ —Value of a cell,  $i, j$ —are layers of a stack,  $\mu$ —is the mean of a layer,  $N$ —is the number of cells,  $k$ —denotes a particular cell [61]

BCS quantifies the relationship between UI and LST, determining the strength and direction of their association. Strong correlations revealed through BCS can inform policy decisions and strategies aimed at enhancing urban sustainability and mitigating urban heat effects.

## 2.7 Variables fuzzification

For decision making with environmental uncertain variables [62] we used fuzzy logic [63, 64] in order to prepare the indicators for further analysis. Fuzzy logic is a multivalued logic that allows intermediate values to be defined between conventional binary evaluations like true/false, yes/no, high/low, etc. [65]. The GIS layer of UI indicators was mathematically analysed in fuzzy logic in ArcGIS with various fuzzy membership functions such as Small, Gaussian, Large, and Linear.

Since we have assumed in our suitability analysis that the highest membership is to be found in our features, we have used the sigmoidal function “fuzzy linear” with the minimum and maximum values given by the user. Everything below the minimum is scored 0 (definitely not a member) and everything above the maximum is scored 1 (definitely a member). A minimum greater than the maximum demonstrates a negative linear relationship (a negative slope). The fuzzy linear function is represented by the following equation:

$$\mu_1(J_1(\lambda(t, K))) = \begin{cases} 1 & , J_1(\lambda(t, K)) < J_1^1 \\ \frac{J_1(\lambda(t, K)) - J_1^0}{J_1^1 - J_1^0} & , J_1^1 \leq J_1(\lambda(t, K)) \leq J_1^0 \\ 0 & , J_1(\lambda(t, K)) > J_1^0 \end{cases}$$

where  $J_1^0$  and  $J_1^1$  are the values of the objective function  $J_1(\lambda(t, K))$  whose degree of membership function are 0 and 1, correspondingly. As one of the possible ways to help the decision maker determine  $J_1^0$  and  $J_1^1$ , to calculate the individual minimum.

$$J_1^{min} = \min_{\lambda(t, K) \in \Lambda(t, K)} J_1(\lambda(t, K)),$$

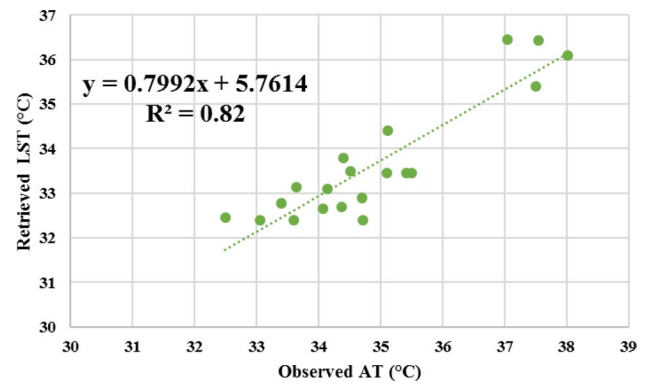
$$J_1^{max} = \max_{\lambda(t, K) \in \Lambda(t, K)} J_1(\lambda(t, K)),$$

Then, considering the calculated individual minimum and maximum of each objective function, the decision maker is asked to assess  $J_1^0$  and  $J_1^1$  in the closed interval  $[J_1^1, J_1^0]$ ,  $i = 1, 2$  [66] (Fig. 4).

## 2.8 Statistical modeling methodology

Path coefficient analysis, a partial least squares (PLS)-based structural equation modeling (SEM) approach, is applied to observed variables to quantify the cause-effect relationship between variables and the mediated relationship of one or more variables for the other contributing variables by systematically inter-connected linear regressions [67]. According to Stage et al. [75], Path analysis is used to calculate estimates of the scale and significance of hypothesized causal

**Fig. 5** Relationship between LST and AT



influences among sets of variables, using path diagrams. The issue in implementing the linear regression analysis method is that we can analyze the relationship between one independent variable and dependent variable and only predict the direct impact of each independent variables on the dependent variable and it is not possible to identify the indirect effects. This method has been used in psychology [68], social sciences [69], business [70], environmental science [71], computer science [72], and medical sciences [73]. In this study, path analysis was used in order to express the effects of the UI parameters on LST. This method is an extension of the regression model that can be used to test the correlation matrix [74] with a fundamental model that can be tested [75]. SPSS software was used to provide path analysis.

## 2.9 SVF calculation

The SVF was calculated in the SAGA-GIS software [76], which is also available as a QGIS plug-in. SAGA-GIS is often used by the urban climate community, for instance, in the framework of the World Urban Data Base and Access Portal Tools (WUDAPT<sup>2</sup>). The algorithm is based on raster input data, where the information on building and terrain vertical elevation is stored in every pixel of the raster, and calculations are performed using two input parameters: the number of directions and the distance of search. The resolution of the raster is also a critical parameter both regarding accuracy and computational duration. It is a major limitation of the algorithm: since a building's footprint is vector-based data, it has to be rasterized in order to be used in SAGA-GIS, thus inducing a loss of information proportional to the raster resolution. [57]

## 2.10 Comparison of thermal behavior of LST

To validate the calculated LST, the AT observations were taken at 19 meteorological stations in Mashhad (Fig. 1b). To reduce the geolocation error of the satellite data, the  $3 \times 3$  homogenous pixels in the sites were selected. The AT observed pattern is similar to LST and the amount of relationship gave validation to LST retrieval which further validates our results. A regression is applied to the relationship between AT and LST and the linear algorithms gave a more validated result with a high  $R^2 = 0.82$  ( $p$ -value  $< 0.001$ ) as shown in Fig. 5. The mean difference (LST-AT) is 5.53 C°, and it confirms that LST is higher than AT. The results show that there is a significant correlation between AT and LST in urban areas. For comparison, Dai et al. [77] report a correlation of  $R^2 = 0.83$  with 18 meteorological stations and LST in Beijing [78]. Sun et al. [78] report a correlation of  $R^2 = 0.93$  for 13 cities in China. These findings suggest that the correlation observed in Mashhad ( $R^2 = 0.82$ ) is comparable to those in other urban areas, demonstrating that the relationship between AT and LST in Mashhad is consistent and reliable.

<sup>2</sup> <http://www.wudapt.org>



### 3 Results

#### 3.1 Spatial distribution of LST

Landsat 8 data is used to estimate the Fraction of Vegetation Cover (FVC) as an indicator of climate change on the environment which includes a combination of bare soil and green vegetation. The spectral properties of these two parameters are usually estimated in different ways, including field measurements, estimates from additional data sources including soil databases and land cover maps, or extracted directly from satellite images.

Figure 6. shows the LST distribution in summer 2022 with calm weather. The maximum LST observed was 63.17 °C and the minimum 31.93 °C. The lowest LSTs are found where trees are abundant. The pattern of LST in Mashhad (Fig. 6) indicates that the hotspots were distributed in the Western, Southern, and Northern areas with the LST more than 40 °C. It shows that gray UI has a higher temperature than green-blue infrastructures including parks and urban green spaces. Also, the barren land cover with bare soil in the West and South, airport and railway stations in the South-east, and agricultural lands in North experience high LSTs. This observation pattern was similar to the results of [79] in Bangkok.

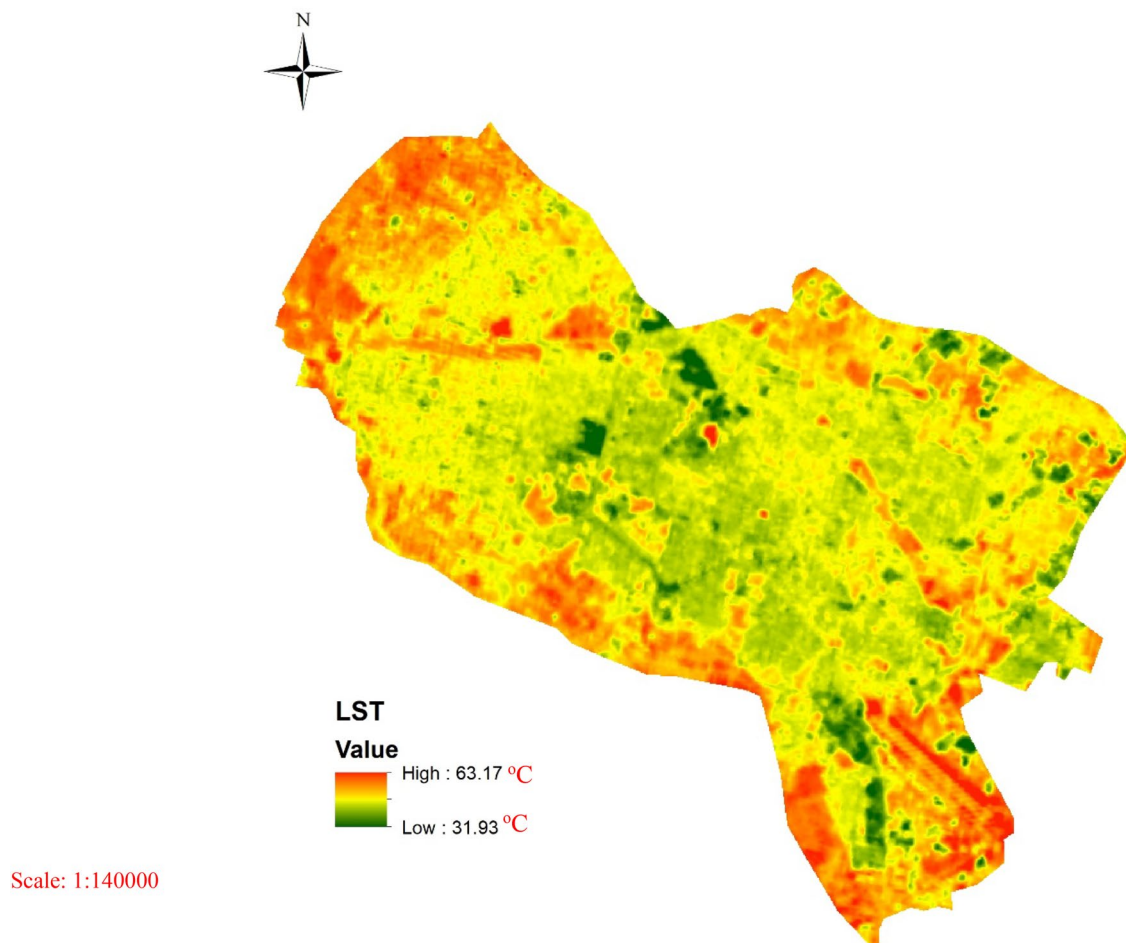


**Fig. 6** Spatial distribution of Land Surface Temperature (LST) in Mashhad on July 22, 2022

### 3.2 UI and LST

In this section, we analyze the impact of various UI layers on LST. The focus is on how different UI layouts and interactive components in the city of Mashhad may influence LST values, contributing to a better understanding of the relationship between urban environments and LST.

#### 3.2.1 UGI and LST

To better understand the relationship between UGI and LST in summer, we extracted data on NDVI, NDMI, and green space area. Each indicator shows varying capacities for reducing LST in Mashhad. The NDVI values in this study range from  $-0.585$  to  $0.849$ , with the highest values located in the city center and northwest areas, where abundant trees and vegetation correlate with lower LST. In contrast, the southern and western areas of the city, characterized by mountainous and barren land, show lower NDVI values. This spatial pattern is evident in the inverse relationship between NDVI and LST, with an  $R^2$  value of  $0.79$  (see Table 4). The NDMI values range from  $0.447$  to  $-0.376$ . The NDMI map shows high moisture levels in the central areas, which contain significant green space with ample tree cover, whereas the south and

**Table 4** UI coefficient of determination with LST in Mashhad

UI	variables	Mean	STD	$R^2$	Relationship
Urban green infrastructure	NDVI	0.170	0.120	0.79	Inverse
	NDMI	0.027	0.063	0.73	Inverse
	Green spaces	0.293	0.298	0.69	Inverse
Urban blue infrastructure	Water well	0.311	0.190	0.64	Inverse
	NDWI	0.143	0.071	0.54	Inverse
	Water channel	0.131	0.174	0.63	Inverse
Urban red infrastructure	Water distribution system	0.036	0.067	0.58	Direct
	Population	0.280	0.186	0.56	Direct
	Families	0.199	0.187	0.44	Direct
Urban gray infrastructure (Land-use)	People in residential units	0.253	0.223	0.60	Direct
	Agriculture	0.028	0.077	0.40	Direct
	Clinical	0.481	0.223	0.61	Inverse
Urban gray infrastructure (urban physical)	Commercial	0.128	0.749	0.42	Direct
	Education	0.072	0.162	0.31	Direct
	Industrial	0.220	0.259	0.46	Direct
	Official	0.129	0.206	0.68	Direct
	Tourism	0.050	0.125	0.34	Direct
	Transportation	0.043	0.151	0.44	Direct
	Barren land	0.177	0.274	0.42	Direct
	Residential	0.083	0.131	0.39	Direct
	Road networks	0.117	0.178	0.53	Direct
	Electricity distribution system	0.026	0.236	0.81	Direct
	NDBI	0.021	0.056	0.61	Direct
	SVF	0.031	0.372	0.51	Inverse
	Building heights	0.095	0.166	0.69	Inverse
	BCR	0.518	0.198	0.53	Inverse
	Wood and adobe	0.070	0.164	0.57	Inverse
	All wood	0.023	0.082	0.39	Direct
	All brick or brick and stone	0.044	0.098	0.49	Direct
	Cinder block	0.063	0.156	0.25	Direct
	Wood and brick or Wood and stone	0.304	0.121	0.27 0.75	Inverse
	Steel and brick or steel and stone	0.280	0.279	0.68	Direct

west exhibit low NDMI due to barren land and the absence of vegetation. Like NDVI, NDMI is inversely correlated with LST, with an  $R^2$  of 0.73. Additionally, areas with higher green space density—particularly in the northeast and north-west—experience noticeably lower temperatures. This inverse correlation between green space area and LST, with an  $R^2$  of 0.69, highlights the significant cooling effect of vegetation density on summer temperatures in Mashhad.

### 3.2.2 UBI and LST

NDWI is proposed for open surface water bodies, which will decrease in the periods of water stress. The calculated NDWI in Mashhad ranges from 0.55 to  $-0.29$ . As expected, the water bodies and waterways present high values of NDWI, compared to other areas. Our results show that the LST has an inverse relationship with NDWI. Mashhad has an arid climate during summer and like other arid cities, to provide water for inhabitants, groundwater reservoirs are reached through wells. In Mashhad the water wells are located mainly in the East and North West of the city and also in the center, where the two expansive gardens with water features are located. The relationship between water wells and LST shows that there is an inverse correlation with value of  $R^2 = 0.64$ . The history of Mashhad shows that there are periods of floods in this city, so there are several channels in Mashhad, both natural and artificial [80], which direct runoff to periurban areas. Although due to climate change the flow of water in these channels is becoming less in terms of volume and frequency, but it still has an inverse effect on LST, equal to  $R^2 = 0.63$ . Water distribution systems have a direct effect on temperature as man-made infrastructure. This network is an artificial feature and mostly made of concrete and PVC, therefore, the relationship is positive with relationship of  $R^2 = 0.58$  with LST.

### 3.2.3 URI relationship with LST

In order to analyze the pattern of population in Mashhad, it is necessary to study the model of zoning system and determine whether the number and extent of settlements in Mashhad city have a uniform and balanced distribution or there is no uniform distribution. If this pattern is clustered, it can also affect the pattern of population accumulation, dispersion and urban growth. This issue has been investigated using the method of the nearest distance, Nearest Neighbor. Case analysis of Y and X and taking into account the coordinates, the results of this analytical tool indicate that the zoning system of Mashhad follows a cluster pattern (Fig S1 in supplementary file-SF). This method of recognizing the spatial patterns of population clustering enables targeted strategies that can address LST. The neighbor number less than 1 indicates that the population is distributed in clusters. The standard score calculated in this case is 54.81, which according to the p-value, we conclude that this clustering is statistically significant. If the mean ratio of the nearest neighbor is less than one, the studied data have a cluster pattern; if it is larger, they have a scattered spatial distribution pattern. The population pattern of Mashhad is clustered and the URI map shows that wherever the population density was higher, the impact on LST was also greater. The coefficient of population, number of households, and households in a residential unit with LST are 0.56, 0.44, and 0.6. Therefore, The URI values and LST have a direct correlation. In other words as the population and the number of households increase in a residential unit the LST value intensifies and increases.

### 3.2.4 UGRI and LST

NDBI is used to show built-up features. There is a strong and positive relationship between NDBI and LST in Mashhad with  $R^2 = 0.61$ . This direct relationship indicates that built-up areas generate more surface temperature and lead to LST intensity in the city. Built-up areas in Mashhad are divided into two categories including urban land-use and urban physical structures. Urban land-use has a direct effect on LST while the urban physical structures demonstrate an inverse effect.

**3.2.4.1 Urban land use relationship with LST** The dominant land-use is classified into 11 classes based on Mashhad LBCS categories (Fig. 2b). Few other land-use classes can be generated but their proportion is too small and does not reflect the variation of LST clearly. The spatial analysis of the city shows that residential land use occupies the large part of the city (7715he), and after that the agriculture (4521.089 he), transportation (437.6 he), education (765.97 he), tourism (396 he), official (120.299 he), clinical (714.151 he), commercial (852.28 he), and public (0.304 he) occupied the lowest area in Mashhad (Mashhad ArcMap layers, 2015). Most of the barren lands in Mashhad area are located in the development zone in the northwest of the city with a total area of 623.47 he. These barren lands mainly are managed with no specific regulation, and are covered with soil and rocks. The results show that land uses in Mashhad have a direct effect on LST except for the clinical land-use. Clinical land use in Mashhad is located in green spaces with abundant trees therefore, the clinical section has an

inverse effect on LST with the  $R^2=0.61$  in this particular city. The relationship between various land use and LST is shown in Fig. 7. Among land uses, the transportation (airport, railways, and bus terminal) and official land use have a strong correlation with LST with  $R^2=0.74$  and  $R^2=0.59$  respectively. Among urban land uses, electricity distribution systems have the greatest impact on LST. This may be due to the fact that most materials used in electricity distribution system are man-made and the relationship with LST is  $R^2=0.81$ .

**3.2.4.2 Urban physical relationship with LST** The height of the buildings in the city varies from 0 (barren lands) to 81m (high rise buildings). Spatial analysis shows that as the height of the buildings increase, the SVF decreases and the buildings shadow leads to lower temperatures. Therefore, there is an inverse association between height of buildings and SVF on LST in Mashhad. The relationship between height of buildings and SVF with LST are  $R^2=0.69$  and  $R^2=0.51$  respectively. Construction materials have also demonstrated an effect on LST. Common construction materials in Mashhad are wood, brick, cement, and iron. Among various building materials clay and brick have an inverse effect on LST with  $R^2=0.57$  and  $R^2=0.49$  respectively. Asphalt has a direct effect on LST with  $R^2=0.63$ .

### 3.3 Spatial analysis of UI and LST

The extracted GIS layers for each indicator were normalized using linear fuzzy for Fuzzy membership function for indicators that construct UGI, UBI, UGRI, and URI in Mashhad. UI was calculated using Fuzzy- Path model for each UI. In order to combine raster layers to find the effect of UI on LST, we used the linear membership. It is used for indefinite phenomena, where if the number is 1 it is a member. Figure 8 shows the spatial analysis combination of green (Fig. 8a), blue (Fig. 8b), red (Fig. 8c) and grey (urban physical, land-use) (Fig. 8d, e) UI indices in the scale of square pixels in the shape of 1000 m\* 1000 m considering the area of neighborhood units for the whole metropolis of Mashhad. UGI in north and center of Mashhad decrease the LST and make it worse in the south where barren lands and airport of Mashhad are located. UBI in center and the north west of the city, mitigate the LST. However, there is a direct pattern with LST and it is clear that as the UBI increases, the LST also increases.

Equation 7. and Fig. 9. show that the slope of the regression is negative, therefore, the UGI values have an inverse relationship with LST. In terms of absolute value of these coefficients, the highest coefficient belongs to the physical dimension and the lowest coefficient to the URI.

$$\text{LST (Mashhad)} = 0.239 + (-0.494 \text{ UGI} + 0.314 \text{ UBI} + 0.394 \text{ urban physical} + 0.248 \text{ Land - use} + 0.225 \text{ URI}) \quad (7)$$

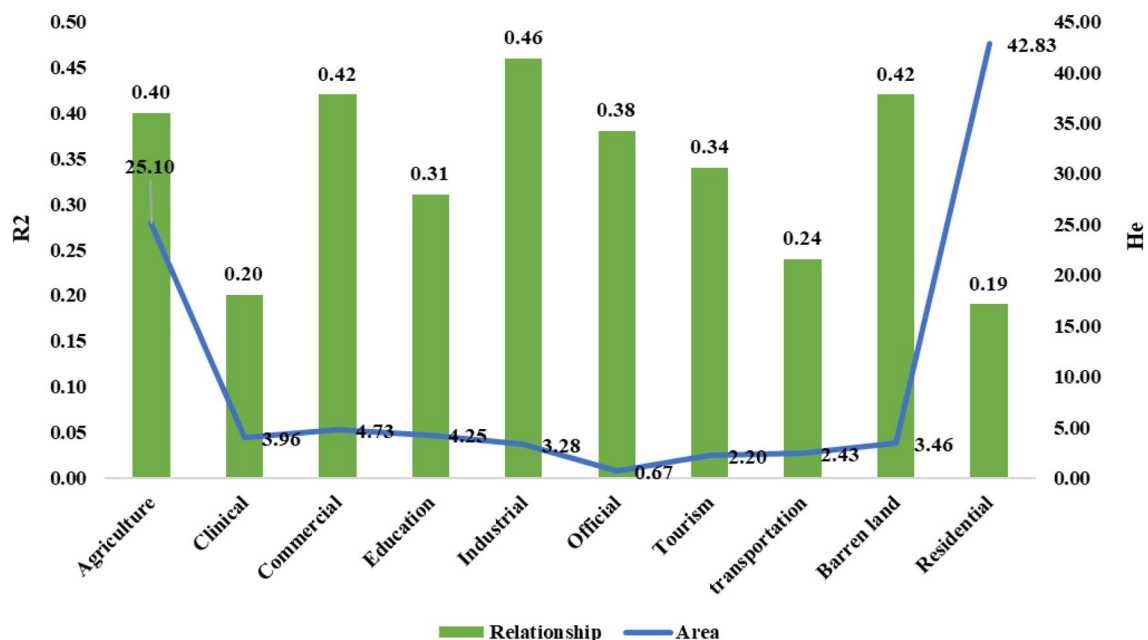
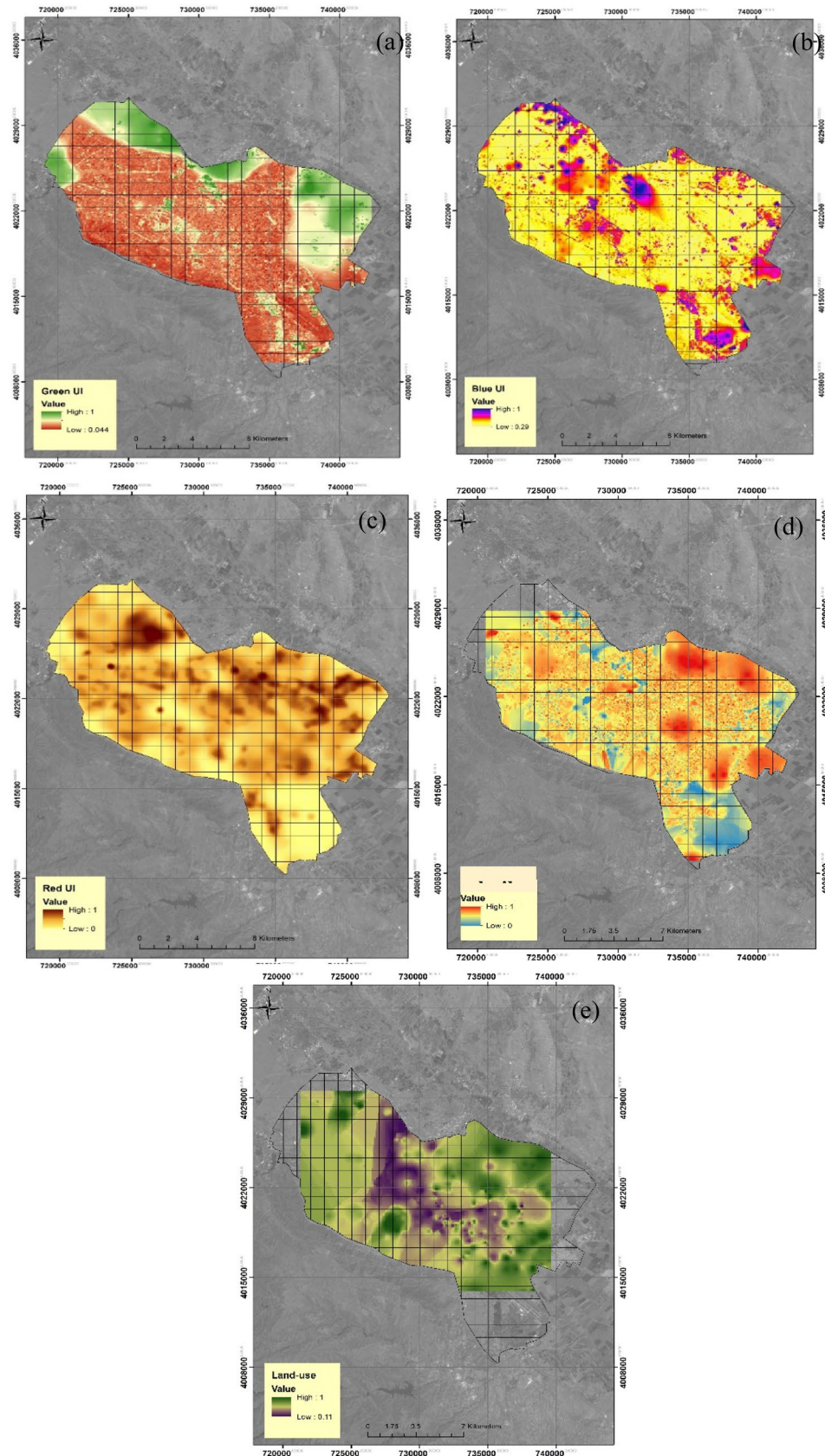


Fig. 7 Relationship between various land use and LST





**Fig. 8** UI layers in Mashhad **(a)** UGI map, **(b)** UBI map, **(c)** URI map, **(d)** urban built up map, **(e)** land use map



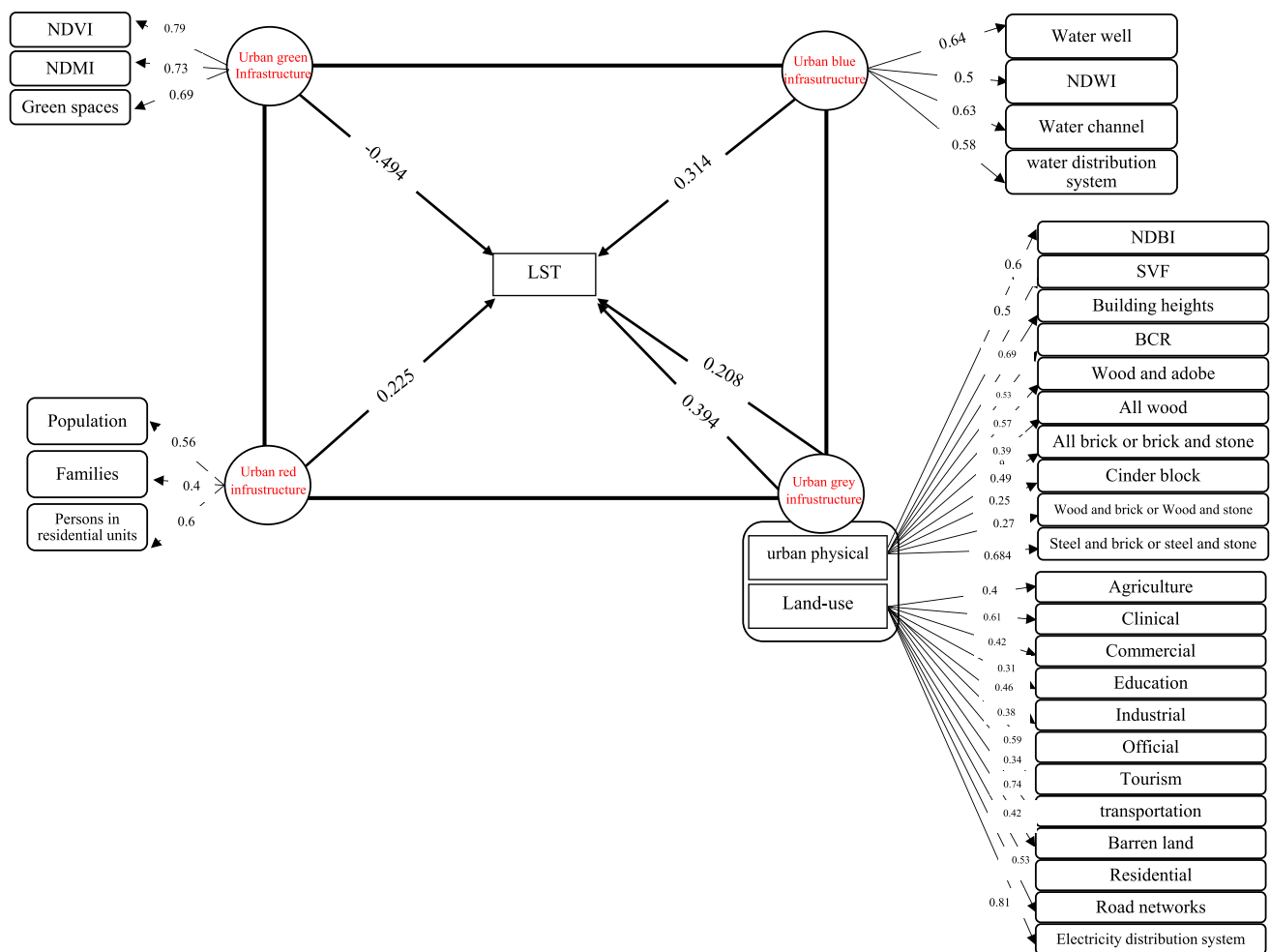


**Fig. 9** Coefficient values of each UI in Mashhad

### 3.4 Summary of the results

The result show that the maximum LST values typically correspond to areas with dense development, limited vegetation, and extensive impervious surfaces. These hotspots often indicate severe UHI effects, where urban areas experience significantly higher temperatures than surrounding rural areas. This information is vital for urban planners to target interventions in these critical zones. Areas with high LST values may correlate with increased health risks, particularly heat-related illnesses. Urban planners can use this information to establish public health interventions, such as increasing access to cooling centers and ensuring vulnerable populations are prioritized in heat response plans. Minimum LST values often occur in areas with abundant vegetation, parks, and water bodies. These regions serve as critical cooling oases within the urban environment. Planners can leverage this data to prioritize the preservation and enhancement of existing green spaces and integrate more greenery into urban design.

- The Landsat 8 data analysis revealed that LST distribution in Mashhad reaches up to 63.17 °C, with hotspots mainly located in the western, southern, and northern regions, particularly where gray infrastructure and barren land cover dominate. The presence of abundant trees in certain areas significantly lowered LST values.
- NDVI, NDMI, and green space area data show that higher vegetation density areas inversely correlate with LST ( $R^2$  values of 0.79, 0.73, and 0.69, respectively). In Mashhad, green spaces with high vegetation, particularly in the center and north, consistently exhibit lower LST values, underscoring the cooling impact of UGI.

- NDWI data indicates that water bodies and water features contribute to lower LST levels, with an inverse correlation of  $R^2=0.64$ . However, artificial water infrastructure (e.g., distribution systems) is positively correlated with LST ( $R^2=0.58$ ), showing that natural UBI elements effectively mitigate heat while engineered water systems may elevate it.
- Population density and household numbers show a direct relationship with LST ( $R^2$  values of 0.56 and 0.6, respectively). The spatial analysis reveals that clustered population zones experience heightened LST levels, suggesting that increased population concentration intensifies heat distribution.

Built-up land and materials are positively correlated with LST (e.g., NDBI with  $R^2=0.61$ ), especially transportation and electricity infrastructure (with high  $R^2$  values of 0.74 and 0.81). Increasing the number and size of parks can significantly reduce LST. Vegetation provides shade and cools the air through evapotranspiration, mitigating the Urban Heat Island (UHI) effect. Clinical land uses, however, show an inverse relationship with LST due to green surroundings. Building height inversely impacts LST due to shadow effects, demonstrating that physical structures contribute variably to urban heat.

- Urban Land Use: High LST in areas dedicated to transportation and official uses; an inverse effect was found in clinical zones, emphasizing that greenery reduces LST ( $R^2=0.61$ ).
- Urban Physical Structures: Taller buildings reduce LST through shading, while materials like asphalt increase it (e.g., direct correlation  $R^2=0.63$  for asphalt).

## 4 Discussion

This study proceeded to analyze UI effects on LST in Mashhad using Fuzzy-Path analysis on various GIS-based indicators. Like other researches e.g. [24, 25, 29, 40, 81, 82], the results of this study showed that UI have effects on LST. By examining the relationship between LST and UI we discovered that this relationship follows a nonlinear correlation and this finding is consistent with Tran et al. [83] studies. The novelty of this work lies in the introduction of the comprehensive concept of UI into GIS modeling. The other aspect of novelty is showing the amount of coefficient of each UI on LST and integration coefficient on LST of Mashhad city. Comparison of LST studies with previous studies e.g. [47, 84] show LST has intensified in the past ten years. Therefore, the indicators of UI affecting LST should be determined more precisely. Previous studies [18] have shown that the normalized difference spectral indices using all combinations of the shortwave infrared (SWIR) bands had stronger correlations with LST than the others in the whole study area. The influence of land-use on LST could be quantified in terms of the percentages of various functions which could potentially be incorporated in planning guidelines. The results show that almost all the UI indicators were interlinked or correlated with LST, therefore, any changes in the UI results is LST variation.

### 4.1 Spatial pattern of LST and red UI

Based on the results of interviews, Social and economic activities of people are the main factors which affect climate change and heat stress. Therefore, significant spatial heterogeneity in the UI-LST association is observed in different types of UI due to the impact of socioeconomic activities and related physical parameters. Diverse socioeconomic activities resulted in different anthropogenic heat patterns, which has an important impact on urban LST [85]. A city with high density experiences more heat stress. Although, the URI coefficient is less than the other UIs, it nevertheless has an impact on LST. The possible explanation is that, as we consider LST during daytime, most people activities occur outside the residential houses, therefore, the amount of human functions consequences on heat production have greater effect than the population density. Thus, we observe the UGRI (land use, urban climate and urban facilities) have higher coefficient in Mashhad.

### 4.2 Spatial pattern of LST and UGI

To measure the effect of UGI on LST, the four spatial models (NDVI, NDWI, NDMI, and green spaces) were resampled at 30 m resolution. The green UI has the strongest correlation with LST [52, 86]. NDVI has a strong positive correlations with NDWI leaf water content, FVC [87] and NDMI. The green spaces covered with tree crowns, grass, and vegetation had a negative correlation with LST. The correlation of green spaces area is weaker than other UGI. The possible explanation is that green spaces in Mashhad have a rather low tree density. Although green spaces are not fully covered by trees

and consist of soil, buildings, roads, and pavements, they still have the negative correlation ( $R^2 = 0.36$ ), yet very weak. To effectively mitigate LST, it is crucial for Mashhad to enhance its tree canopy cover with a higher density of trees and a medium to high Leaf Area Index (LAI). These results are consistent with the study by Bartesaghi-Koc et al. [88], showing that UGI has a significant effect on LST [88].

### 4.3 Spatial pattern of LST and UBI

Previous studies showed the negative effect of water bodies on LST [40]. However, our results for Mashhad for water network distribution and seasonal rivers are positive. This can be explained by the fact that Mashhad has an arid climate in summer, when the seasonal rivers are dry and the soil is exposed. The water distribution network is an artificial feature, mostly made of concrete and PVC, therefore, the relationship is positive. In spite of the low area of the water pits, the correlation is negative with LST. One reason for this is the size of the water body, deeper and larger are more effective on LST. However, the combination of the UBI layers coefficient still has lower effect on surface temperature.

### 4.4 Spatial pattern of LST and UGRI

Both land-use (2D building) [89] and urban physical structures (3D building morphology) [89] indicators can affect the partitioning of the energy balance and can therefore modify the urban microclimate and thermal conditions [90]. The results indicate UGRI plays an important role on LST in Mashhad.

Agricultural land covered more than 25% of the study area, and temperatures were comparable to built-up areas. The soil and preparation of the fields lead to higher LST in this city. The heat generated in office and commercial buildings during the day coincides with the cluster area with high LST, which shows that energy consumption in this building types is generally an important source of urban warming. Since the study of residential buildings in this research is during the day and the interactions with these buildings mostly happen at night [91], the effectiveness of residential buildings during the day is less than commercial buildings. In our studies, it has been shown that road networks have a positive relationship with LST, which could be due to the dark asphalt covering. Dark asphalt absorbs solar radiation, stores the heat and increases the LST. On the other hand, the movement of vehicles and the heat produced by them are other reasons [92]. There is also considerable LST differences between built-up and barren lands [93]. In our studies the barren lands experience higher LST correlation. One possible reason is the barren land is covered with soil and rock that rise the LST. Therefore, in the city of Mashhad, LST is reduced by using lands mixed with green space and abundant trees. These results are consistent with the study by Moazzam et al. [94], showing that LST alteration is impacted by urban areas [94].

The variation in building height is among the most influential indicators to LST [95]. This indicator pattern is related to SVF pattern and BCR and the results indicate a negative correlation with LST. The possible explanation might be, although the 3D building morphology places more emphasis on building landscape, which changes the physical surface properties such as specific heat capacity and evapotranspiration efficiency [96], a positive relationship with barren lands indicates that the built-up areas bring cooler situation to the city, and the 3D building morphology can indicate the building's shadow, materials, and SVF and incident solar radiation. Therefore, the correlation between 2D building morphology and LST was weaker than 3D buildings. Lower SVF in areas with taller buildings means more shading, which can significantly reduce solar radiation access [97] and therefore reduce surface temperatures and enhance temperature in dense urban settings. By planning for varying building heights in areas with high pedestrian traffic, urban designers can naturally cool environments, reducing the intensity of urban heat islands (UHIs). This approach can be particularly effective in cities with hot climates, where shaded streetscapes contribute to cooler, more comfortable public spaces. A more comprehensive effort in UI studies during the night and comparing day and night effects on LST is suggested for future studies.

By understanding which UI elements contribute most significantly to LST, urban planners can prioritize interventions like increased green and blue infrastructure in heat-prone areas. For example, planners might use this data to design zoning regulations that require green spaces in residential and commercial developments, particularly in densely populated and high-traffic areas. Additionally, planners can integrate water features and strategically plant trees in hotspots to mitigate LST, especially around transportation hubs and barren land areas.

Vegetation and water bodies not only reduce LST but also improve air quality. Plants act as natural filters, absorbing pollutants like carbon dioxide, nitrogen dioxide, and particulate matter. As temperature rises, pollutant dispersion can worsen, so strategically placed green infrastructure helps mitigate these effects, improving overall air quality and potentially reducing respiratory issues in densely populated areas. The distribution of green and blue spaces often

correlates with social and economic factors within cities, influencing residents' quality of life. An inverse relationship between UI and LST that considers social equity is crucial, as it encourages equitable access to cooler, healthier environments across all urban areas. Ensuring that green infrastructure reaches underserved areas can help reduce social disparities in health outcomes and overall urban experience.

## 5 Conclusion

This study shows a comprehensive UI combination effect on LST with path analysis using fuzzy-path analysis methods, hotspot analysis using Getis Ord  $G_i^*$  statistics and band correction statistics to investigate the relationship between UI and LST intensity. Fuzzy-path analysis accommodates the complex, often nonlinear relationships between UI factors and LST, capturing the uncertainty and variability inherent in urban environments more effectively than rigid, traditional models. Getis Ord  $G_i^*$  statistics precisely identify spatial “hot” and “cold” spots, allowing planners to pinpoint specific areas with elevated or reduced temperatures. This localized approach offers more actionable insights than broader, averaged analyses. Results from this study provide an effective methodology for characterizing UHI and have significant implications for policy makers and communities by providing an empirical basis for climate change mitigation programs for urban planners and designers. By examining the relationship between LST and UI we discovered that this relationship follows a nonlinear correlation and this finding is consistent with Tran et al. [83] studies. We found that hotspot analysis using Getis Ord  $G_i^*$  statistics is an appropriate method to examine changes in LST patterns through time. Identifying hot and cold spots in urban areas is crucial for understanding the dynamics LST in relation to UI. Hot spots—areas with significantly elevated temperatures—often correlate with urban features such as dense development, limited vegetation, and impervious surfaces, which contribute to the Urban Heat Island (UHI) effect. Conversely, cold spots—areas with lower temperatures—are frequently associated with green spaces, water bodies, and urban design elements that promote cooling. The identification of hotspot or coldspot areas by such method does not depend on whether the mean surface temperature is high or low. In our research, the coefficient of determination ( $R^2$ ) is approximately 0.4 in some cases. While this value may initially appear modest, it is crucial to consider the complex context of our study, which focuses on urban environments. Cities are dynamic systems influenced by a myriad of interrelated factors and confounding variables, making it challenging to capture the full extent of relationships with a single model. In the context of urban research, where numerous unpredictable and interacting elements are at play, an  $R^2$  of 0.4 provides meaningful insight and demonstrates a noteworthy level of explanatory power. This result underscores the importance of our findings and highlights the relevance of our model in understanding urban climate phenomena amidst the inherent complexity of city environments. This paper completes the previous studies which do not consider Red UI and interactive UI effects on LST. Among UI parameters, UGRI (land-use, urban physical) has the most effective coefficient on LST in Mashhad. Therefore, as the land-uses mixed with green space and abundant trees (like clinical land-use in Mashhad), the LST decreases. This situation becomes better in locations with more shading from buildings and trees with various crowns. Moreover, attention should be devoted to UGI in order to decrease the barren lands area and UGRI effects on LST. Findings highlight the vital need for contextual policies for UHI mitigation strategies tailored to the urban grey infrastructure. The methodology used in this paper can be evaluated in other cities worldwide. Transferring the findings of this study to other urban contexts involves careful consideration of several influencing factors, as each city's unique characteristics and climate conditions impact the relationship between urban infrastructure (UI) and Land Surface Temperature (LST). A further study is suggested to investigate the impact of UI on UHI, considering a time series to assess whether the thermal behaviour persists over time.

**Acknowledgements** Tash Consulting provided ArcGIS layers for the Mashhad Municipality

**Author contributions** Conceptualization, E.SD and D.MP; methodology E.SD and D.MP; software E.SD; formal analysis, E.SD and E.S; investigation, E.SD; writing—original draft preparation, E.SD; writing—review and editing, D.MP, E.S, S.A.; visualization, E.SD; All authors have read and agreed to the published version of the manuscript.

**Funding** This research did not have the courtesy of any funding from any organization.

**Data availability** The raw data presented in his study are available on request. The data are not publicly available due to privacy.

## Declarations

**Ethics approval and consent to participate** Research on human-related subjects is reviewed by individual departments within the university. The study was conducted in accordance with the University of Shahrood's guidelines, under approval number DM/1005.

**Consent for publication** All named authors in the paper agree to submit the manuscript for publication.

**Informed consent** Informed consent was obtained from all participants involved in the study. The authors affirm that participants were fully informed about the study's purpose, potential risks, and expected benefits.

**Competing interests** The authors declare no competing interests.

**Open Access** This article is licensed under a Creative Commons Attribution-NonCommercial-NoDerivatives 4.0 International License, which permits any non-commercial use, sharing, distribution and reproduction in any medium or format, as long as you give appropriate credit to the original author(s) and the source, provide a link to the Creative Commons licence, and indicate if you modified the licensed material. You do not have permission under this licence to share adapted material derived from this article or parts of it. The images or other third party material in this article are included in the article's Creative Commons licence, unless indicated otherwise in a credit line to the material. If material is not included in the article's Creative Commons licence and your intended use is not permitted by statutory regulation or exceeds the permitted use, you will need to obtain permission directly from the copyright holder. To view a copy of this licence, visit <http://creativecommons.org/licenses/by-nc-nd/4.0/>.

## References

1. Nations U. Department of Economic and Social Affairs, Population Division. World Population Prospects 2019: Highlights. ST/ESA/SER.A/423. 2019.
2. Wang W, Wu T, Li Y, Xie S, Han B, Zheng H, et al. Urbanization impacts on natural habitat and ecosystem services in the Guangdong-Hong Kong-Macao "Megacity." *Sustainability*. 2020;12(16):6675.
3. Aflaki A, Mirnezhad M, Ghaffarianhoseini A, Ghaffarianhoseini A, Omrany H, Wang Z-H, et al. Urban heat island mitigation strategies: a state-of-the-art review on Kuala Lumpur Singapore and Hong Kong. *Cities*. 2017;62:131–45.
4. Shahmohamadi P, Che-Ani AI, Maulud KNA, Tawil NM, Abdullah NAG. The impact of anthropogenic heat on formation of urban heat island and energy consumption balance. *Urban Stud Res*. 2011;2011:497524.
5. Lee TW, Lee JY, Wang Z-H. Scaling of the urban heat island intensity using time-dependent energy balance. *Urban Climate*. 2012;2:16–24.
6. Santamouris M. Regulating the damaged thermostat of the cities—status, impacts and mitigation challenges. *Energy Build*. 2015;91:43–56.
7. Santamouris M. Cooling the cities—A review of reflective and green roof mitigation technologies to fight heat island and improve comfort in urban environments. *Sol Energy*. 2014;103:682–703.
8. Santamouri M, Asimakopoulou D, Assimakopoulou VD, Chrisomallidou N, Klitsikas N, Mangold D, et al. Energy and climate in the urban built environment 2013. 1–402 p.
9. Tan J, Zheng Y, Tang X, Guo C, Li L, Song G, et al. The urban heat island and its impact on heat waves and human health in Shanghai. *Int J Biometeorol*. 2010;54(1):75–84.
10. Weng Q. Thermal infrared remote sensing for urban climate and environmental studies: methods, applications, and trends. *ISPRS J Photogramm Remote Sens*. 2009;64(4):335–44.
11. Lu L, Weng Q, Xiao D, Guo H, Li Q, Hui W. Spatiotemporal variation of surface urban heat islands in relation to land cover composition and configuration: a multi-scale case study of Xi'an, China. *Remote Sens*. 2020;12(17):2713.
12. Radhi H, Sharples S, Assem E. Impact of urban heat islands on the thermal comfort and cooling energy demand of artificial islands—A case study of AMWAJ Islands in Bahrain. *Sustain Cities Soc*. 2015;19:310–8.
13. Xue J, You R, Liu W, Chen C, Lai D. Applications of local climate zone classification scheme to improve urban sustainability: a bibliometric review. *Sustainability*. 2020;12(19):8083.
14. Arif N, Khasanah AN, Jaya R, Gozan M, Hendrawan B. The effect of land surface temperature and land use on energy system development in Gorontalo City. *J Phys: Conf Ser*. 2019;1179:012103.
15. Mashhoodi B. Land surface temperature and energy expenditures of households in the Netherlands: Winners and losers. *Urban Climate*. 2020;34:100678.
16. Roa-Espinosa A, Wilson T, Norman J, Johnson K. Predicting the impact of urban development on stream temperature using a thermal urban runoff model (TURM). *Proc, US EPA National Conf on Urban Stormwater: Enhancing Programs at the Local Level*. 2003.
17. Dickinson RE, Henderson-Sellers A, Kennedy PJ, Wilson MF. Biosphere-atmosphere Transfer Scheme (BATS) for the NCAR Community Climate Model (No. NCAR/TN-275+STR). University Corporation for Atmospheric Research; 1986.
18. Alexander C. Normalised difference spectral indices and urban land cover as indicators of land surface temperature (LST). *Int J Appl Earth Obs Geoinf*. 2020;86:102013.
19. Pal S, Ziaul S. Detection of land use and land cover change and land surface temperature in English Bazar urban centre. *Egypt J Remote Sens Space Sci*. 2017;20(1):125–45.
20. Despini F, Ferrari C, Santunione G, Tommasone S, Muscio A, Teggi S. Urban surfaces analysis with remote sensing data for the evaluation of UHI mitigation scenarios. *Urban Climate*. 2021;35:100761.
21. Yao L, Xu Y, Zhang B. Effect of urban function and landscape structure on the urban heat island phenomenon in Beijing China. *Landsc Ecol Eng*. 2019;15(4):379–90.



22. Yazdani S, Yusof MJM, Azizi MM, Ali AAA. Effects of lack of coordination in the context of urban infrastructure provision: a multiple embedded case study in Iran. *Int J Manag Sci.* 2015;6(6):291–303.
23. Ness DA. Sustainable urban infrastructure in China: towards a Factor 10 improvement in resource productivity through integrated infrastructure systems. *Int J Sustain Dev World Ecol.* 2008;15:288–301.
24. Zölch T, Rahman MA, Pfeleiderer E, Wagner G, Pauleit S. Designing public squares with green infrastructure to optimize human thermal comfort. *Build Environ.* 2019;149:640–54.
25. Nastran M, Kobal M, Eler K. Urban heat islands in relation to green land use in European cities. *Urban For Urban Green.* 2019;37:33–41.
26. Marando F, Salvatori E, Sebastiani A, Fusaro L, Manes F. Regulating ecosystem services and green infrastructure: assessment of urban heat island effect mitigation in the municipality of Rome Italy. *Ecol Model.* 2019;392:92–102.
27. Chun B, Guldman J-M. Impact of greening on the urban heat island: seasonal variations and mitigation strategies. *Comput Environ Urban Syst.* 2018;71:165–76.
28. Aleksandrova K. Green, grey or green-grey? Decoding infrastructure integration and implementation for residential street retrofits. Minneapolis: Lincoln University; 2016.
29. Grilo F, Pinho P, Aleixo C, Catita C, Silva P, Lopes N, et al. Using green to cool the grey: modelling the cooling effect of green spaces with a high spatial resolution. *Sci Total Environ.* 2020;724:138182.
30. Pauleit S, Fryd O, Backhaus A, Jensen MB. Green Infrastructure green infrastructure climate change green infrastructure and climate change-climate change. In: Loftness V, Haase D, editors. *Sustainable built environments*. New York: Springer New York; 2013. p. 224–48.
31. Brudermann T, Sangkakool T. Green roofs in temperate climate cities in Europe—an analysis of key decision factors. *Urban For Urban Green.* 2017;21:224–34.
32. Maheng D, Ducton I, Lauwaet D, Zevenbergen C, Pathirana A. The sensitivity of urban heat island to urban green space—a model-based study of City of Colombo, Sri Lanka. *Atmosphere.* 2019;10(3):151.
33. Kumar P, Druckman A, Gallagher J, Gatersleben B, Allison S, Eisenman TS, et al. The nexus between air pollution, green infrastructure and human health. *Environ Int.* 2019;133:105181.
34. Vieira J, Matos P, Mexia T, Silva P, Lopes N, Freitas C, et al. Green spaces are not all the same for the provision of air purification and climate regulation services: the case of urban parks. *Environ Res.* 2018;160:306–13.
35. Oke TR. The energetic basis of the urban heat island. *Quart J Meteorol Soc.* 1982;108(445):1–24.
36. Völker S, Baumeister H, Claßen T, Hornberg C, Kistemann T. Evidence for the temperature-mitigating capacity of urban blue space—A health geographic perspective. *Erdkunde.* 2013;67:355–71.
37. Kim YH, Ryoo SB, Baik JJ, Park IS, Koo HJ, Nam JC. Does the restoration of an inner-city stream in Seoul affect local thermal environment? *Theor Appl Climatol.* 2008;92(3):239–48.
38. Saaroni H, Ziv B. The impact of a small lake on heat stress in a Mediterranean urban park: the case of Tel Aviv Israel. *Int J Biometeorol.* 2003;47:156–65.
39. Kalinowska MB. Effect of water–air heat transfer on the spread of thermal pollution in rivers. *Acta Geophys.* 2019;67(2):597–619.
40. Wu C, Li J, Wang C, Song C, Chen Y, Finka M, et al. Understanding the relationship between urban blue infrastructure and land surface temperature. *Sci Total Environ.* 2019;694:133742.
41. Vojinovic Z, Keerakamolchai W, Weesakul S, Pudar RS, Medina N, Alves A. Combining ecosystem services with cost-benefit analysis for selection of green and grey infrastructure for flood protection in a cultural setting. *Environments.* 2017;4(1):3.
42. Alves A, Sanchez A, Vojinovic Z, Seyoum S, Babel M, Brdjanovic D. Evolutionary and holistic assessment of green-grey infrastructure for CSO reduction. *Water.* 2016;8(9):402.
43. Boarnet MG, Forsyth A, Day K, Oakes JM. The street level built environment and physical activity and walking: results of a predictive validity study for the irvine minnesota inventory. *Environ Behav.* 2011;43(6):735–75.
44. Hao T, Rogers CDF, Metje N, Chapman DN, Muggleton JM, Foo KY, et al. Condition assessment of the buried utility service infrastructure. *Tunn Undergr Space Technol.* 2012;28:331–44.
45. Pramanik S, Punia M. Land use/land cover change and surface urban heat island intensity: source–sink landscape-based study in Delhi, India. *Environ Dev Sustain.* 2020;22(8):7331–56.
46. Habibi N, Masnavi M, Malekmohamadi B. Ecological landscape design of urban rivers with emphasis on Run—Off Water Control ( Case study: Ziyarat Gorgan river ). *J Environ Stud.* 2018;43(4):609–29.
47. Naserikia M, Asadi Shamsabadi E, Rafeian M, Filho W. The urban heat island in an urban context: a case study of Mashhad Iran. *Int J Environ Res Pub Health.* 2019;16:313.
48. Soltanifard H, Aliabadi K. Impact of urban spatial configuration on land surface temperature and urban heat islands: a case study of Mashhad Iran. *Theor Appl Climatol.* 2019;137(3):2889–903.
49. Baaghdeh M, Mayvaneh F. Climate change and simulation of cardiovascular disease mortality: a case study of Mashhad Iran. *Iran J Pub Health.* 2017;46(3):396–407.
50. Asghar Pil Hoor A, Pourahmad A. The process of growth and development of the country's metropolises Case study: (Mashhad city). 2005;48:103–21.
51. Jiménez-Muñoz JC, Sobrino JA, Skoković D, Mattar C, Cristóbal J. Land surface temperature retrieval methods from landsat-8 thermal infrared sensor data. *IEEE Geosci Remote Sens Lett.* 2014;11(10):1840–3.
52. Dai Z, Guldman J-M, Hu Y. Spatial regression models of park and land-use impacts on the urban heat island in central Beijing. *Sci Total Environ.* 2018;626:1136–47.
53. Conrad O, Bechtel B, Bock M, Dietrich H, Fischer E, Gerlitz L, et al. System for automated geoscientific analyses (SAGA) v. 2.1.4. *Geosci Model Dev.* 2015;8(7):1991–2007.
54. Rouse JW, Haas RH, Schell JA, Deering DW. Monitoring vegetation systems in the great plains with ERTS.: Symposium-Volume I: Technical Presentations. NASA, Washington, D.C; 1973.
55. Mcfeeters SK. The use of normalized difference water index (NDWI) in the delineation of open water features. *Int J Remote Sens.* 1996;17:1425–32.

56. Gao BC. NDWI—a normalized difference water index for remote sensing of vegetation liquid water from space. *Remote Sens Environ.* 1996;58:257–66.
57. Bernard J, Bocher E, Petit G, Palominos S. Sky view factor calculation in urban context: computational performance and accuracy analysis of two open and free GIS tools. *Climate.* 2018;6(3):60.
58. Landsat NASA. Science Data Users Handbook 2017. <http://landsat.usgs.gov/l8handbook.php>. Accessed 23 Sep 2015.
59. Chavez PS. An improved dark-object subtraction technique for atmospheric scattering correction of multispectral data. *Remote Sens Environ.* 1988;24(3):459–79.
60. Moran PAP. Notes on continuous stochastic phenomena. *Biometrika.* 1950;37(1/2):17–23.
61. ESRI. Esri: GIS Mapping Software, Location Intelligence & Spatial analytics 2016. [www.pro.arcgis.com](http://www.pro.arcgis.com).
62. Heuvelink GBM, Brown JD. Uncertain environmental variables in GIS. In: Shekhar S, Xiong H, editors. *Encyclopedia of GIS*. Boston: Springer, US; 2008. p. 1184–9.
63. Zadeh LA. Fuzzy sets. *Inf Control.* 1965;8(3):338–53.
64. Zadeh LA. Fuzzy algorithms. *Inf Control.* 1968;12(2):94–102.
65. Sharma EM. A survey in fuzzy logic: an introduction. 2014.
66. Sakawa M. Prediction and operational planning in district heating and cooling systems. Amsterdam: Elsevier; 2016.
67. Neo SM, Choong WW, Ahamad RB. Differential environmental psychological factors in determining low carbon behaviour among urban and suburban residents through responsible environmental behaviour model. *Sustain Cities Soc.* 2017;31:225–33.
68. Ayala-Rojas RE, Granero R, Mora-Maltas B, Rivas S, Fernández-Aranda F, Gómez-Peña M, et al. Factors related to the dual condition of gambling and gaming disorders: a path analysis model. *J Psychiatr Res.* 2022;145:148–58.
69. Dong B, Krohn MD. The effects of parental school exclusion on offspring drug use: an intergenerational path analysis. *J Crim Just.* 2020;69:101694.
70. Bao MX, Cheng X, Smith D. A path analysis investigation of the relationships between CEO pay ratios and firm performance mediated by employee satisfaction. *Adv Account.* 2020;48:100457.
71. Xu D, Zhang Y, Li Y, Wang X, Yang Z. Path analysis for carbon transfers embodied in China's international trade and policy implications for mitigation targets. *J Clean Prod.* 2022;334:130207.
72. Wang Q, Zhang G, Sun C, Wu N. High efficient load paths analysis with U\* index generated by deep learning. *Comput Methods Appl Mech Eng.* 2019;344:499–511.
73. Siegmund LA, Distelhorst KS, Bena JF, Morrison SL. Relationships between physical activity, social isolation, and depression among older adults during COVID-19: a path analysis. *Geriatr Nurs.* 2021;42(5):1240–4.
74. Spaeth JL. Path analysis: Introductory multivariate analysis. In: Amick DJ, Walberg HJ, editors. *ImaFe, psychological, and social research*. Berkeley: McCutchan; 1975.
75. Stage F, Carter H, Nora A. Path analysis: an introduction and analysis of a decade of research. *J Educ Res J Educ Res.* 2004;98:5–13.
76. Böhner J, McCloy KR, Strobl J. SAGA: analysis and modelling applications. Göttingen: Goltze; 2006.
77. Dai Z, Guldman J-M, Hu Y. Thermal impacts of greenery, water, and impervious structures in Beijing's Olympic area: a spatial regression approach. *Ecol Ind.* 2019;97:77–88.
78. Sun T, Sun R, Chen L. The trend inconsistency between land surface temperature and near surface air temperature in assessing urban heat island effects. *Remote Sens.* 2020;12:1271.
79. Adulkongkaew T, Satapanajaru T, Charoenhirunyingyos S, Singhirunnusorn W. Effect of land cover composition and building configuration on land surface temperature in an urban-sprawl city, case study in Bangkok Metropolitan Area, Thailand. *Heliyon.* 2020;6(8):e04485.
80. Hosseinzadeh Seyed R, Jihadi TM. Effects of Mashhad city expansion on the pattern of natural drainage and intensification of urban floods. *Geogr Res.* 2007;39(61):145–59.
81. Lin Y, Wang Z, Jim CY, Li J, Deng J, Liu J. Water as an urban heat sink: Blue infrastructure alleviates urban heat island effect in mega-city agglomeration. *J Clean Prod.* 2020;262:121411.
82. Sturiale L, Scuderi A. The role of green infrastructures in urban planning for climate change adaptation. *Climate.* 2019;7:119.
83. Tran DX, Pla F, Latorre-Carmona P, Myint SW, Caetano M, Kieu HV. Characterizing the relationship between land use land cover change and land surface temperature. *ISPRS J Photogramm Remote Sens.* 2017;124:119–32.
84. Gorgani S, Panahi M, Rezaie F. The Relationship between NDVI and LST in the urban area of Mashhad, Iran. 2013.
85. Yang J, Wang Y, Xiu C, Xiao X, Xia J, Jin C. Optimizing local climate zones to mitigate urban heat island effect in human settlements. *J Clean Prod.* 2020;275:123767.
86. Weng Q, Lu D, Schubring J. Estimation of land surface temperature–vegetation abundance relationship for urban heat island studies. *Remote Sens Environ.* 2004;89(4):467–83.
87. Gu Y, Brown JF, Verdin JP, Wardlaw B. A five-year analysis of MODIS NDVI and NDWI for grassland drought assessment over the central Great Plains of the United States. *Geophys Res Lett.* 2007. <https://doi.org/10.1029/2006GL029127>.
88. Bartesaghi-Koc C, Osmond P, Peters A. Spatio-temporal patterns in green infrastructure as driver of land surface temperature variability: the case of Sydney. *Int J Appl Earth Obs Geoinf.* 2019;83:101903.
89. How Jin Aik D, Ismail MH, Muharam FM. Land Use/land cover changes and the relationship with land surface temperature using landsat and MODIS imageries in cameron highlands Malaysia. *Land.* 2020;9(10):372.
90. Tian L, Li Y, Lu J, Wang J. Review on urban heat Island in China: methods, its impact on buildings energy demand and mitigation strategies. *Sustainability.* 2021;13(2):762.
91. Shafran-Nathan R, Yuval, Broday DM. Impacts of personal mobility and diurnal concentration variability on exposure misclassification to ambient pollutants. *Environ Sci Technol.* 2018;52(6):3520–6.
92. Neog R, Lahkar B, Baruah J, Acharjee S, Gogoi BS, Sonowal B, et al. An infrared thermography-based study on the variation in diurnal and seasonal land surface temperature at Dibrugarh city India. *Model Earth Syst Environ.* 2020;6(4):2047–61.
93. Sadiq Khan M, Ullah S, Sun T, Rehman AU, Chen L. Land-use/land-cover changes and its contribution to urban heat Island: a case study of Islamabad, Pakistan. *Sustainability.* 2020;12(9):3861.

94. Moazzam MFU, Doh YH, Lee BG. Impact of urbanization on land surface temperature and surface urban heat Island using optical remote sensing data: a case study of Jeju Island Republic of Korea. *Build Environ.* 2022;222:109368.
95. Sun F, Liu M, Wang Y, Wang H, Che Y. The effects of 3D architectural patterns on the urban surface temperature at a neighborhood scale: relative contributions and marginal effects. *J Clean Prod.* 2020;258:120706.
96. Jamei E, Rajagopalan P. Urban development and pedestrian thermal comfort in melbourne. *Sol Energy.* 2017;144:681–98.
97. Xu M, Hong B, Jiang R, An L, Zhang T. Outdoor thermal comfort of shaded spaces in an urban park in the cold region of China. *Build Environ.* 2019;155:408–20.

**Publisher's Note** Springer Nature remains neutral with regard to jurisdictional claims in published maps and institutional affiliations.